J. Comput. Appl. Res. Mech. Eng. Vol. 12. No. 2, pp. 193-209, 2023 DOI: 10.22061/JCARME.2022.8268.2101

SRTTU

Journal of Computational and Applied Research in Mechanical Engineering

jcarme.sru.ac.ir

JCARME

ISSN: 2228-7922

Research paper

Experimental investigation and modeling of fiber metal laminates hydroforming process by GWO optimized neuro-fuzzy network

A. H. Rabiee[a] , E. Sherkatghanad[b], A. Zeinolabedin Beygi[b], H. Moslemi Naeini[b,*] and L. Lang[c]

[a] *Department of Mechanical Engineering, Arak University of Technology, Arak, Iran*
[b] *Department of Mechanical Engineering, Tarbiat Modares University, Tehran, Iran*
[c] *Department of Industrial and Manufacturing System Engineering, Beihang University, Beijing, China*

Article info:

Article history:

Received: 22/07/2021
Accepted: 06/05/2022
Revised: 08/05/2022
Online: 10/05/2022

Keywords:

Neural network;
ANFIS;
Gray wolf algorithm;
Hydroforming;
Fiber metal laminates.

***Corresponding author:**
moslemi@modares.ac.ir

Abstract

In this paper, by considering the processing parameters, including blank holder force, blank holder gap, and cavity pressure as the most important input factors in the hydroforming process, an experimental design is performed, and an adaptive neural-fuzzy inference system (ANFIS) is applied to model and predict the behavior of aluminum thinning rate (upper layer and lower layer), the height of wrinkles and achieved depths that are extracted in hydroforming process. Also, the optimal constraints of the network structure are obtained by the gray wolf optimization algorithm. Accordingly, the results of experimental tests are utilized for training and testing of the ANFIS. The accurateness of the attained network is examined using graphs and also based on the statistical criteria of root mean square error, mean absolute error, and correlation coefficient. The results show that the attained model is very effective in approximating the aluminum thinning rate (upper layer and lower layer), the height of wrinkles, and achieved depth in the hydroforming process. Finally, the results also show that the root means of the square error of aluminum thinning rate (upper layer and lower layer), the height of wrinkles, and achieved depth of the test section are 1.67, 2.25, 0.05, and 2.67, respectively. It is also observed that the correlation coefficient for the test data is very close to 1, which demonstrates the high precision of the ANFIS in predicting the outputs of the hydroforming procedure.

1. Introduction

Metal–composite structures, also named fiber metal laminate (FML) materials made of alternative strata, including fiber composite layers and metals, joined through resin films. These hybrid structures as materials can be utilized in different required properties using different materials of constituents. FMLs as hybrid materials present superior results than the simple sum of their separate effects and have superior resistance to fatigue, mechanical characteristics, damage tolerance, thermal characteristics, and enhanced environmental shelter [1-7]. FMLs and usual composite materials have been validated as successful selection and applied in the aerospace industry

as well as the military sector because of outstanding fatigue resistance as well as the impact characteristics [8]. Furthermore, towards increasing energy productivity and decreasing perilous releases in transport automobiles, investigation in advanced lightweight materials is a prevalent research area [9, 10]. Due to the progress in advanced materials like FMLs, the attention to applying these parts to produce new products is increasing several times [11-13]. As depicted in Fig. 1, different types of lightweight materials are being utilized in the aerospace industry to manufacture parts like fuselage panels. Even in this time, due to the time-consuming production methods, limited applications can be found for FMLs as the compound materials, especially in mass production like automobile and building industries, as well as commercial end-user goods. The authors believe that hydroforming as a conventional production technique applied in different industries can be suitable for FMLs and offers a capable production way to make high-volume products. Finding a high-volume production method which is proper for fiber netal laminates by applying the hydroforming technique needs to study. Also, the material behavior during the forming is needed to investigate in detail.

Usually, monolithic materials such as metal alloys possess a big strain at failure, which is about 10-50%, but composite materials have constrained elongation. In fact, the strain at failure for fibers is around 1%, 2-2.5%, and between 4 to 5% for carbon, aramid, and glass fibers, respectively. The resins' strain at failure, especially for thermoplastic-based polymers, is also limited [14]. GLARE, ARALL, and CARAL are the trade name of fiber metal laminates using carbon fibers, glass, and aramid in the middle layers, respectively. These kinds of materials have been graded for different applications in aerospace structures. GLARE material has thin strata of aluminum which are fixed and bound to uni-directional or multi-directional high strength fibers of glass which has been pre-impregnated. This material, which is the base material in this study, offers a pioneering mixture of features such as outstanding resistance to fatigue, superior static characteristics, significant resistance to impact, etc. Also, for usual parts and those parts which are not complicated, production and repair are not complex. This material has been designated for Airbus A380 in the upper fuselage coating and was the first request of GLARE materials in a marketable air company [15]. Using GLARE material, different collections of the FMLs were made. These parts have the ability to avoid and break the progress of tracks produced by dynamically loading. Also, it has admirable characteristics like impact tolerance, although its density is low and specific strength and stiffness are high.

Due to the long-time production of FML parts, limited consumption of these kinds of materials (FMLs) is available, especially while mass-volume products are needed. In order to obtain satisfactory mass-volume products using fiber metal laminates utilizing the hydroforming process, understanding the drawing performance is vital [15, 16]. Actually, the hydro-deep drawing and hydroforming technique is a standard industrial procedure employed in many sectors and provides effective manufacturing systems to fabricate high-volume products. Finding straight forming for FML products can improve fabrication speeds several times quicker, compared with current production methods. Inquiries show hydro-bulging forming as the usual and useful testing method to investigate uniform materials, especially sheet metals [17, 18] and has rarely been applied for FMLs. Two main approaches have been utilized for the manufacturing of GLARE as a fiber metal laminate.

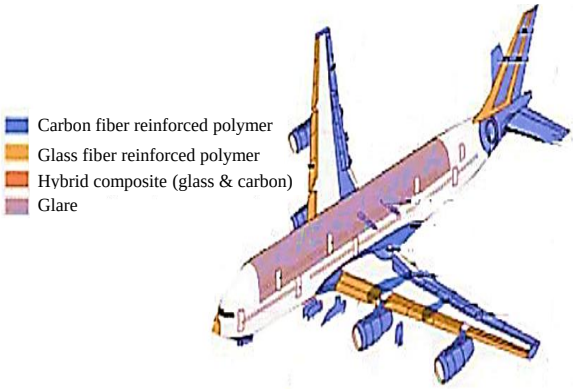

Fig. 1. Light-weight materials in Boeing 787 Dreamliner [15].

The first manufacturing process is constructed by applying autoclaves especially to make big parts such as airplane parts. The above-mentioned process considers the most common method due to its quality and consistency [19, 20]. Although by autoclave method, the quality of the final part can be better, some limitations such as lengthy production time as well as operational prices make its usage challengeable, especially in the mass-volume products [21, 22]. The alternative technique is using FML as the blank to form. Before developing our proposed method, only FML materials having the middle layer with polypropylene-based resins (PP) filled with chopped fibers, could employ to produce FML laminates by applying conventional forming [23-25]. In addition to the above-mentioned approaches, there is a fresher process entitled vacuum injected molding or VARTM which means vacuum assisted resin transfer molding. Actually, in this system, the resin can flow between the layers to create a joint between them. So in this process. inter-laminar characteristics can be enhanced. Recently, theoretical studies on forming treating have been gradually industrialized to be used in practical aspects, especially for unsolved problems or complex problems. This tendency is particularly evident in the development of smart structures, which are usually subjected to experimental records. Artificial neural network (ANN) is a part of the system that transfers knowledge and rules contained in experimental data to the structure of their processed network. Because artificial neural networks do not make any prior assumptions about data characterization and statistical distribution, they are practically more efficient than conventional statistical methods. Generally, ANNs are not able to create a model at a logical time. Furthermore, a fuzzy logic system requires a way to learn from experimental data to exert integrated rules from different variables. Consequently, considering the advantages and disadvantages of both approaches, the successful combination of these methods has created neural-fuzzy modeling. Due to the importance of determining the parameters of the hydroforming process and also the wide application of neural-fuzzy modeling in the field of mechanical engineering, in this paper, the effect of the parameters of the hydroforming process is investigated. In recent years, several researches have been used to model various engineering processes by using the ANFIS system [26-28]. Dadgar asl *et al.* [29] used ANN-based genetic algorithm II to attain the parameters of the flexible roll forming processing. Esfahani *et al.* [30] developed a method for determining the optimized density of the mesh according to a adaptive network-based fuzzy inference system, to predict the deflection caused by the scanning of the circular path of the laser beam considering analysis time and forming accuracy. Maji *et al.* [31] worked on the optimization of incremental forming parameters using the response surface method and models based upon ANFIS structure, in order to reach the wanted figure with optimum formability. Khamneh *et al*. [32] used the design of experiment to calculate the spring back of creep aged formed AA7075 with a statistical analysis. The variance analysis showed that temperature is more important than other parameters. Safari *et al.* [33] used the design of experiment according to the response surface approach, and extracted the governing linear regression equation for spring-back of the creep age formed fiber metal laminates.

In the present paper, an ANFIS network is utilized to model the significant parameters in the hydroforming process of Fiber Metal Laminates, Blank Holder Force, Blank Holder Gap, and Cavity Pressure, for predicting aluminum thinning rate (upper layer and lower layer), the height of wrinkles and achieved depth. For this purpose, the results of experiments performed to train and test the ANFIS structure have been utilized. Moreover, to attain the optimal topology of the model, the gray wolf algorithm has been used.

2. Methodology

2.1. Materials and properties

To find an efficient forming approach, primarily, it is necessary to understand the forming behavior of both GLARE and its constituents simultaneously.

Table 1. Mechanical properties of aluminum 2024-T [13, 14, 19]

Material	Density (g/cc)	Yield stress (MPa)	UTS (MPa)	Anisotropy (r)	Strain hardening exponent (n)	E (GPa)	Elongation (%)
2024-T3	2.78	298	425	0.780	0.195	73	19.2

Table 2. Mechanical properties of unidirectional carbon fibers and prepreg woven glass fibers [13, 14, 19]

Type of fiber	Density (g/cc)	Thickness (mm)	Tensile strength (MPa)	Tensile modulus (GPa)	Shear modulus (MPa)	Elongation (%)
Plain weave of glass fiber	2.55	0.2	800	30	4.2	4.8
Unidirectional of carbon	1.8	0.2	3500	130	4.4	1.8

In order to achieve this goal, many related works have been investigated, and many experiments have been done.Generally, GLARE materials under tension offer an inelastic performance because of the plasticity of aluminum sheets. Therefore, the modulus of elasticity of all kinds of GLAREs must be slightly poorer than the uniform Al-alloy because of the low modulus of elasticity in prepreg laminates. GLAREs with unidirectional prepregs in the middle clearly demonstrate powerful characteristics directionally. The prepregs cause superior properties such as stiffness, modulus, and strength along with their orientation, at the same time, metallic sheets govern the tensile characteristics in the perpendicular path. As it is obvious the behavior is much more complicated than a monolithic material. The mechanical properties of the constituent, such as aluminum 2024-T, unidirectional carbon fibers, and Prepreg woven glass fibers are depicted in Tables 1 and 2.

2.2. Simulation principles

The finite element software, ABAQUS/Explicit, and Dynaform were employed to carry out the finite element simulation analysis. The properties parameters of the aluminum alloy and glass fiber materials obtained from the mechanical properties experiments were input into the simulation software material property module. All the molds are regarded as rigid bodies. The four-node grid elements are used for punch, the concave molds, and the blanking ring. Each layer material is a double-curvature shell element deformable body, but it is for laminates. In the case of the aluminum alloy layer, it is regarded as the elastoplastic material model, nut in the next section, and the glass fiber and carbon fiber layers are regarded as the lamina. In fact, the different characteristics are formulated, the values are 0.15, 0.1, and 0.05, and in the case of FMLs coefficient of friction can be varied between 0.1-0.5. The friction functions to form multilayer parts is pretty intricate due to the existence of further interaction between the blank's interlayers. Actually, in the Fiber Metal Laminates, the experimental forces of punch are higher than that of the numerical values, particularly in the deep drawing, because of the larger frictional forces through the tests than expected for the numerical study. Blanks of aluminum alloys are considered a circular form with a diameter of 140 mm, a punch radius is 37.5 mm, and die radius is 40 mm.

It needs to be mentioned that for the simulations in Abaqus software, aluminum is considered an isotropic material, and anisotropy is neglected. In the present study, to consider the anisotropic influence of the aluminum alloy, the 36*MAT_3PARAMETER_BARLAT code of Dynaform/LS Dyna has been chosen in simulations for obtaining FLDs of aluminum and multilayer aluminum blanks in the software, but in other simulations, the materials considered as quasi-isotropic. ABAQUS, in this study, is applied to simulate the behavior of the GLARE material. Besides, DYNAFORM/LS-DYNA is employed for the simulation of multilayer parts.

Table 3. Parameters of FML components used in numerical simulations in the lamina situation [13, 14, 19]

Material	Density (g/cc)	E1 (GPa)	E2 (GPa)	Poisson ratio (ν_{12})	G12 (GPa)	G23 (GPa)	G13 (GPa)
Aluminum 2024-O	2.72	73.1	73.1	0.33	28.0	28.0	28.0
Carbon fiber	1.76	232.0	8.61	0.25	3.75	2.30	2.30
Glass fiber	2.52	53.98	9.412	0.13	3.50	2.06	2.06

For FML analysis, two layers of the aluminum laminates are considered as isotropic and meshed, so one layer of fabric was meshed utilizing this software, and laminate properties input the software as mentioned in Table 3 for each layer in the lamina condition. In this case, all of the needed parameters are given in the table. So, the material properties shown in Table 3 are put into the material attribute module of the simulation software. At the same time, the Hashin failure criterion is used to judge the failure mode of composite materials. In this case, 6 parameters are needed, which are provided by the supplier of the material.

To simulate the process, the punch, binder, and die have been entirely constrained, whereas the punch just can travel through the Z-axis path. Also, the contact interface was used to make the alternating interaction and sliding boundary conditions among the metallic layers as well as the tools and sheets. The friction coefficient among the punch and blank was considered 0.15, and 0.1 for the binder and the blank, respectively, and 0.05 for the die and the blank, but the real one may depend on the existence of the lubricant material in that place. The coefficient of friction between the FML blank layers depends on the nominal friction for each contact which depends on the curing stage from 0.15 to 0.5. In some experiments, it is tried to make a situation the same as simulations assumptions by using lubricants. The general numerical simulation setup model using is depicted in Fig. 2.

Several experiments and simulation were done to investigate the present innovative method, and they are discussed here. In the experimental condition, as depicted in Fig. 3, and three aluminum blanks with 0.5 mm thickness (total thickness = 1.5 mm) have been formed concurrently at the cavity pressures of 40 MPa, where the gap was kept fixed. One of the most important reasons is the larger frictional forces called as dry friction force appearing from contacts of the blanks interlayer in the case of the 3-layer blank. The wrinkling zone was monitored previously the optimum failure zone and cavity pressure and happened after as the optimum cavity pressure amount. In fact, this test is the first gate to understanding the material properties when we have 3 separated layers.

As the main idea of this research will be focused on the multilayer and laminated material, investigating the three aluminum layers can give important results to find a way for FMLs to form. So, an investigation has been done on the stress distributions in every layer. Abaqus is the employed software in this sector, while Dynaform has been used in the case of obtaining FLD of single-layer and multi-layer aluminum blanks. In this sector, the anisotropy of aluminum has been neglected.

As shown in Fig. 4, stress distributions are investigated for each layer. The result for the optimum parameters is shown. The maximum Mises stress in the whole layers is approximately equal, just a little different. All of the contacts are between metallic layers, and the formability of each layer is considerable. It is clear that for FMLs the forming situation is completely different and complicated, but it is the first step to the main goal.

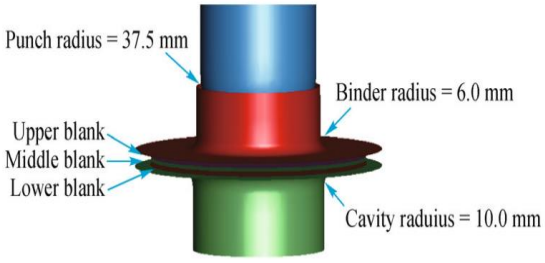

Fig. 2. General numerical simulation setup model.

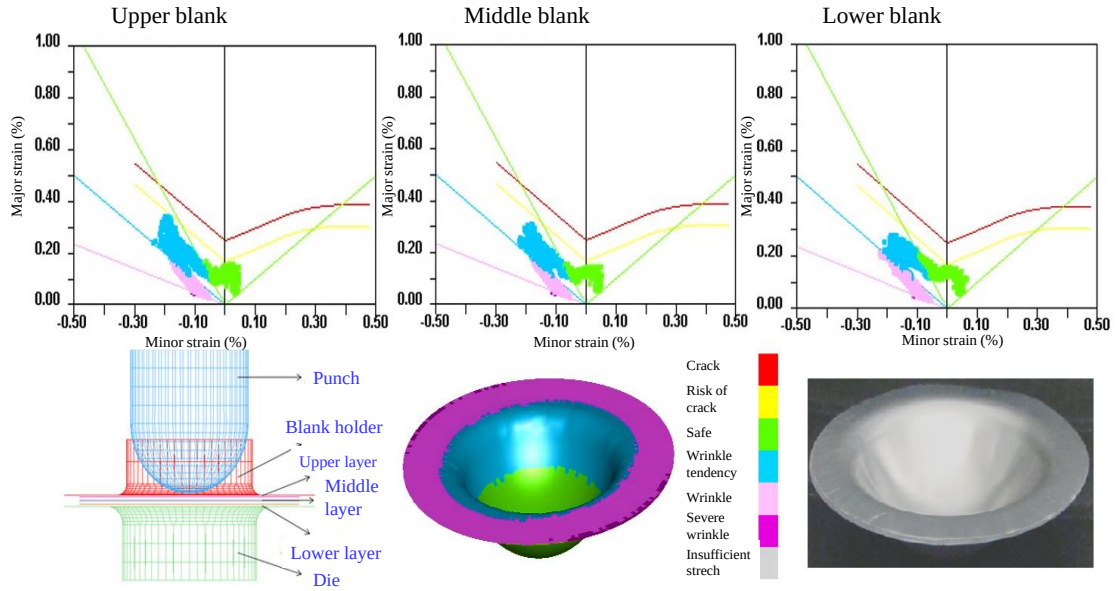

Fig. 3. Numerical simulation and experimental results for blank style-3 at the cavity pressure of 40 MPa.

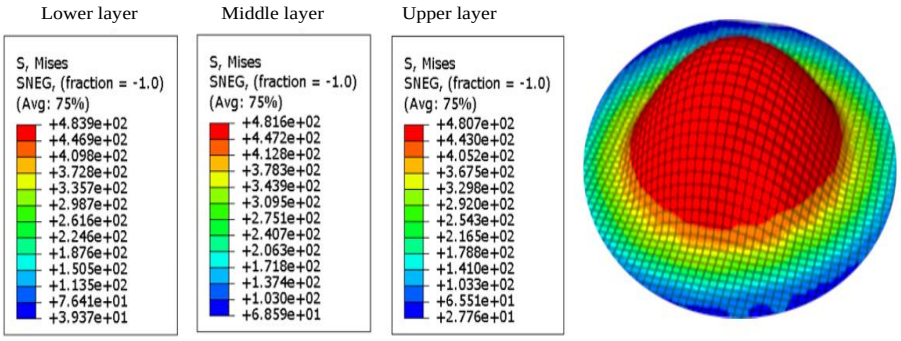

Fig. 4. Stress distributions in three-layer aluminum blank.

As depicted in the above figure, due to the more deformation in the lower layer, bigger stress is presented, but as the properties of the whole layers are the same, there is no big difference between them. The lowest stress relates to the upper layer, and the bigger one relates to the lower layer. In this case, the stress in the middle layer is between the upper and lower. Another reason for equal stiffness may be due to the same coefficient of friction between metallic parts, while in the FML materials, everything will be different even by using semi-cured FMLs.

2.3. Experimental method

Table 4 presents the intended inputs along with the test results. The values of the output variables for each of the 24 experiments are given.

3. Optimized intelligent modeling

3.1. ANFIS structure

The ANFIS model benefits from two methods of artificial neural networks (ANN) and fuzzy inference systems (FIS). Like FISs, the ANFIS includes double sections, the preliminary and the consequence, which are linked by specific fuzzy rules. ANFIS includes five layers, which define this network as a multilayer ANN structure. The Takagi-Sugeno Fuzzy models as one kind of this network have double inputs and a single output, which is shown in Fig. 5.

This network consists of inputs x and y and output f which are linked based on the rules:

Rule 1: If (x equals A_1) and (y equals B_1), then it becomes $f_1 = p_1 x + q_1 y + r_1$

Table 4. Experiments performed and outputs response values.

Specimens	Factors			Evaluation index			
	BHG [mm]	BHF [KN]	CP [MPa]	Al thinning rate [%] experimental		Height of wrinkles [mm]	Depth achieved [mm]
				Upper	Lower		
1	1	4	2.5	14.00	18.00	0.0	24
2	1	6.50	6	14.40	19.30	0.0	21
3	1	8	8	14.70	20	0.0	19
4	1	9	10	15. 0	20.7	0.0	17
5	1	11.50	15	16.00	21.10	0.0	14
6	1	13	18	17.00	21.50	0.0	12
7	1.05	4	6	10.00	14.00	0.0	31
8	1.05	6.50	2.5	10.7	14.20	0.0	31
9	1.05	8	8	11.00	15	0.0	32
10	1.05	9	15	11.20	16.00	0.0	34
11	1.05	11.50	10	11.50	16.50	0.0	36
12	1.05	13	18	11.50	16.00	0.0	33
13	1.1	4	10	3.8	4.40	0.4	27
14	1.1	6.50	15	3.8	4.50	0.3	27
15	1.1	8	8	4.00	4.70	0.2	27
16	1.1	9	2.5	4.30	5.00	0.10	26
17	1.1	11.50	6	4.50	5.30	0.10	26
18	1.1	13	18	4.0	5.0	0.1	26
19	1.15	4	15	3.30	4.00	0.80	26
20	1.15	6.50	10	3.60	4.50	0.50	26
21	1.15	8	8	3.70	4.50	0.4	26
22	1.15	9	6	4.00	5.00	0.40	26
23	1.15	11.50	2.5	4.00	5.30	0.25	23
24	1.15	13	18	3.50	5.00	0.2	20

Rule 2: If (x equals A_2) and (y equals B_2), then it becomes $f_2 = p_2x + q_2y + r_2$

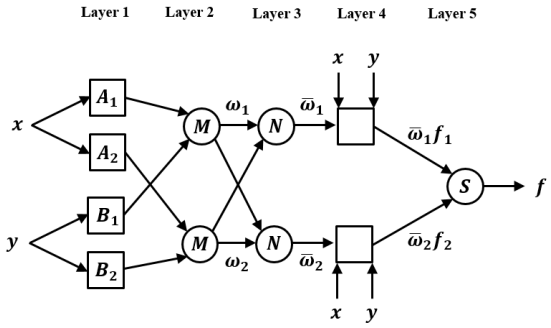

Fig. 5 ANFIS network structure.

In this system, A_i and B_i are distinguished as the sets of FIS and f are the network output. Moreover, p_i, q_i, r_i are parameters which are achieved through the training procedure. If the outcome of each layer is defined as o^i_i , then the characteristics of the layers can be described as follows:

Layer 1: Each node is related to a fuzzy set and its outcome is equal to the membership function (MF) degree of the related input. The form of the MFs is specified by the corresponding parameters of that node. If the Gaussian membership functions are utilized, one can attain:

$$\mu_{Ai}(x) = e^{-\frac{1}{2}\left(\frac{x-c_i}{\sigma_i}\right)^2} \quad (1)$$

where c_i and σ_i are the center and width of the membership functions, respectively.
Layer 2**:** Here, the inputs are multiplied and the strength of the rule firing is written as follows:

$$O_i^2 = \omega_i = \mu_{Ai}(x)\mu_{Bi}(y), \qquad i = 1,2 \quad (2)$$

where μ_{Bi} is the degree of MF of *y* in the fuzzy set B_i, and $\mu_{Ai}$is the degree of MF of *x* in the fuzzy set A_i.
Layer 3: The nodes calculate the weight of the if-then rules, in which ω_i^n is the normalized fire strength.

$$O_i^3 = \omega_i^n = \frac{\omega_i}{\omega_1 + \omega_2} \qquad i = 1,2 \quad (3)$$

Layer 4: This layer is recognized as the rule layer, which is attained by multiplying the output of the third layer in the outcome of the Takagi-Sugeno system.

$$O_i^4 = \omega_i^n f_i = \omega_i^n(p_i x + q_i y + r_i), \qquad i = 1,2 \quad (4)$$

Layer 5: The last layer, consists of a node in that all the inputs of the node are gathered together:

$$O_i^5 = \sum_{i=1}^{2} \omega_i^n f = \frac{\omega_1 f_1 + \omega_2 f_2}{\omega_1 + \omega_2}, \qquad i = 1,2 \quad (5)$$

It is noted here that the first and fourth layers are adaptive layers where c_i and σ_i known as parameters related to the input MFs. In the fourth layer r_i, q_i, and p_i are adaptive parameters identified as output parameters. Recently, numerous metaheuristic optimization algorithms have been utilized to rise the efficiency of the ANFIS. Gray wolf algorithm is one of the newest and most effectual approaches which is utilized here to optimize the ANFIS structure.

3.2. Gray wolf optimization algorithm

The nature-inspired gray wolf optimization algorithm (GWO), is developed by Mirjali *et al.* [34], and considered in the group of the population-based optimization algorithms. The general advantages of the GWO algorithm over other algorithms include less cost and storage computational necessities, easier implementation, simpler structure, faster convergence speed, and fewer adjustable parameters used in the algorithm. Gray wolves have a dominant social hierarchy, as shown in Fig. 6. The leaders of the group are a female and a male named alpha. The second level in the gray wolf hierarchy is beta. Beta wolves are secondary ones that help with alpha in decisions or other group events. Delta wolf must report to Alpha and Beta but dominates Omega. Omega has the lowest rank, and should always obey the other wolves. The GWO algorithm, like the Particle Swarm optimization algorithm, starts from a random population. In each iteration, the alpha, beta, and delta members renew their situation according to their prey location. This update also endures until the space between the wolves and the prey is stopped or a satisfactory result is achieved. In GWO, alpha wolves are the finest solution. Other wolves tracks are based on their dominion. Specifically, the gray wolf algorithm consists of the following steps:
Stage 1: The initial population of gray wolves is randomly created. The created crowd is characterized by the n-dimensional search space for operating *M* locations. To repeat, start with *k* = 0 initialization and continue to k_{max}.

$$P_j(k) = [P_j^1(k).....P_j^f(k).....P_j^n(k)]^T,\ j \in \{\alpha, \beta, \delta\} \quad (6)$$

where $k = 1,2,...,k_{\max}$ are the present iteration numbers, k_{max} is the maximum iteration, and $P_\alpha(k), P_\beta(k), P_\delta(k)$ is the solutions vector.
Stage 2: The performance of each wolf is examined based on the accuracy of the approximation of the experimental data of the present problem. Evaluating the performance of each member leads to the value of the fitness function that is used for the GWO optimization algorithm using: $P_i(k) = \rho,\ i = 1,2,...,M$

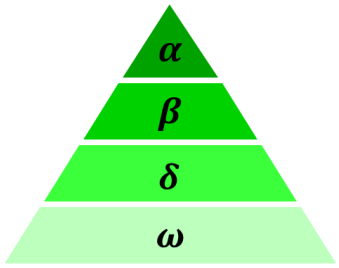

Fig. 6. The hierarchy of gray wolfs.

Stage 3: The three best solutions $P_\alpha(k), P_\beta(k), P_\delta(k)$, are identified by:

$$J(P_\alpha(k)) = \min_{i=j,..,M}\{J(P_i(k)), P_i(k) \in D_p\}, \quad (7)$$

$$J(P_\beta(k)) = \min_{i=j,..,M}\{J(P_i(k)), P_i(k) \in D_p / P_\alpha(k)\}, \quad (8)$$

$$J(P_\delta(k)) = \min_{i=j,..,M}\{J(P_i(k)), P_i(k) \in D_p / P_\alpha(k), P_\beta(k)\}, \quad (9)$$

The solution condition is defined as follows:

$$J(P_\alpha(k)) < J(P_\beta(k)) < J(P_\delta(k)) \quad (10)$$

Stage 4: Here, the search vector coefficients are obtained utilizing Eqs. (11 and 12):

$$R_j(k) = [r_j^1(k)....r_j^f(k)....r_j^n(k)]^T \quad (11)$$

$$S_j(k) = [s_j^1(k)....s_j^f(k)....s_j^n(k)]^T, j \in \{\alpha,\beta,\delta\}, \quad (12)$$

in which:

$$r_j^f(k) = r^f(k)(2q^f - 1), \quad (13)$$

$$s_j^f(k) = 2q^f, j \in \{\alpha,\beta,\delta\}, \quad (14)$$

where q^f the uniform distribution of a random value in the range $0 \le q^f \le 1, f = 1...n$ and the constant $r^f(k)$ in the search process is reduced from 2 to 0.

$$r^f(k) = 2[1-(k-1)/(k_{\max}-1)], f = 1...n \quad (15)$$

Stage 5: Here, the constant agents are permitted to catch their new position.

$$V_j^i(k) = \left|S_j^f(k)P_j^f(k) - P_i^f(k)\right|, \quad i = 1...M, j \in \{\alpha,\beta,\delta\} \quad (16)$$

By attaining notation $P^j(k)$ for renewed Alpha, Beta, and Delta solutions:

$$P^j(k) = [p^{j1}(k)...p^{if}(k)...x^{jm}(k)]^T, j \in \{\alpha,\beta,\delta\} \quad (17)$$

The components of these solutions are as follows:

$$P^{if}(k) = p_j^f(k) - r_j^f(k)v_j^i(k), f = 1...n, i = 1...M, j \in \{\alpha,\beta,\delta\} \quad (18)$$

And the updated solution vector $P_i(k+1)$ is calculated by Eq. *X*:

$$P_i(k+1) = (P^\alpha(k) + P^\beta(k) + P^\delta(k))/3, i = 1...M. \quad (19)$$

Stage 6: The renewed solution $P_i(k+1)$ is validated by the objective function.

Stage 7: The GWO algorithm is redone from step 2 till the repetition k eaches the maximum value from the initial value.

Stage 8: In the last stage, the algorithm stops and the finest solution ever found is saved as:

$$\rho^* = \arg\min_{i=1...M} J(P_i(k_{\max})) \quad (20)$$

4. Results and discussion

In this study, there are 24 laboratory data for network testing and testing, including three inputs blank holder force (BHF), blank holder gap (BHG), and cavity pressure (CP), and four outputs aluminum thinning rate (upper layer and lower layer), the height of wrinkles and achieved depth. This set of data is randomly separated into two subsets, 70% for training and 30% for testing. Figs. 7-10 show the optimized Gaussian membership functions for the output aluminum thinning rate (upper layer and lower layer), the height of wrinkles, and achieved depth, respectively.

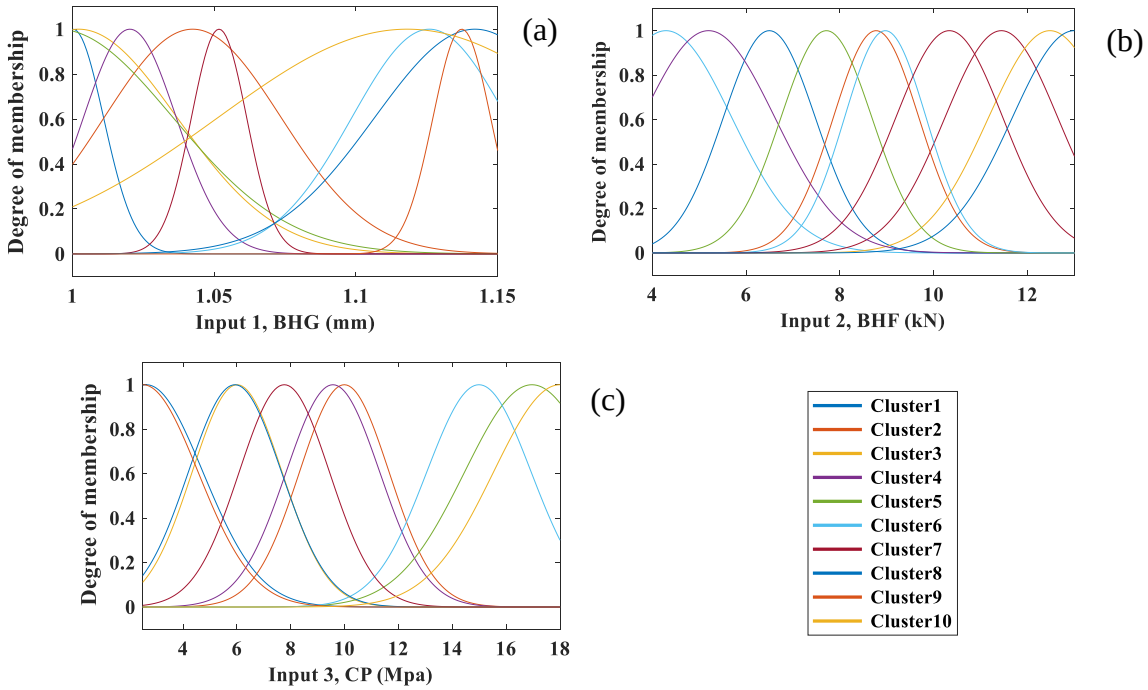

Fig. 7. Optimized membership functions for aluminum thinning rate in upper layer; (a) Input 1, (b) Input 2 and (c) Input 3.

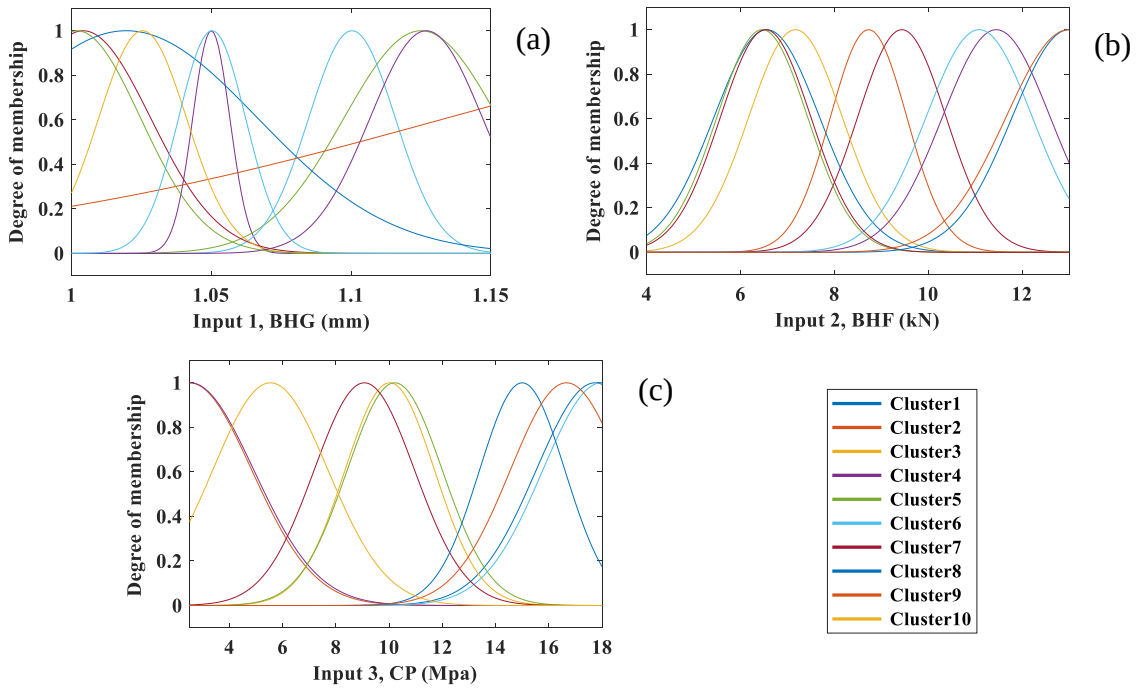

Fig. 8. Optimized membership functions for aluminum thinning rate in lower layer; (a) Input 1, (b) Input 2 and (c) Input 3.

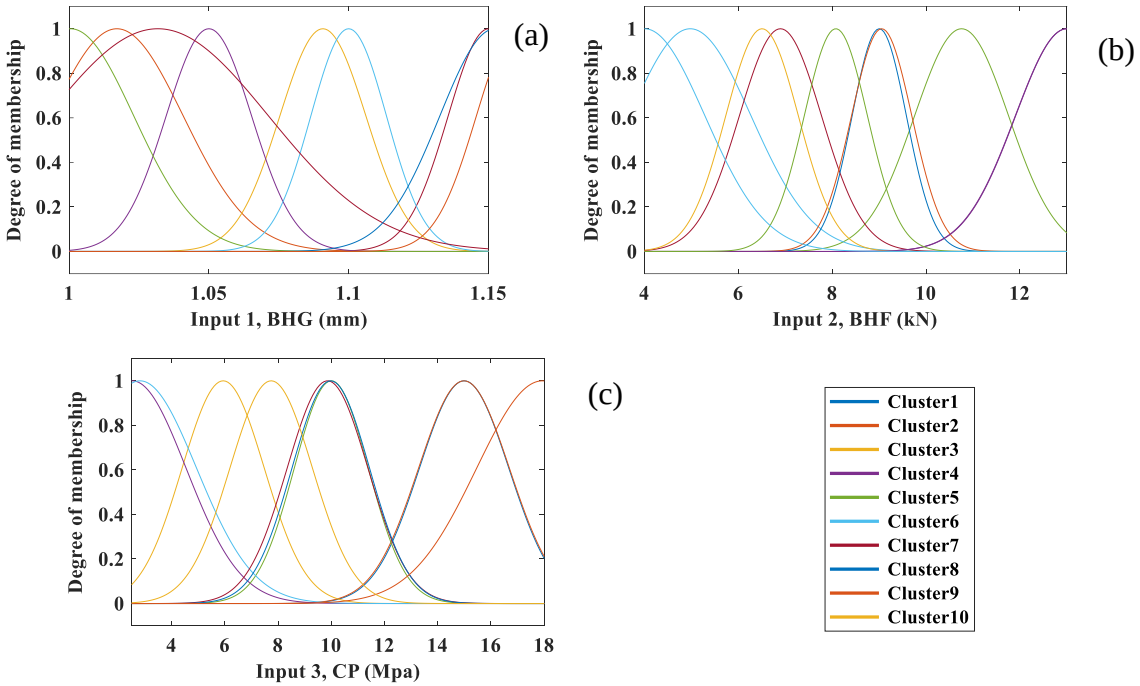

Fig. 9. Optimized membership functions for height of wrinkles; (a) Input 1, (b) Input 2 and (c) Input 3.

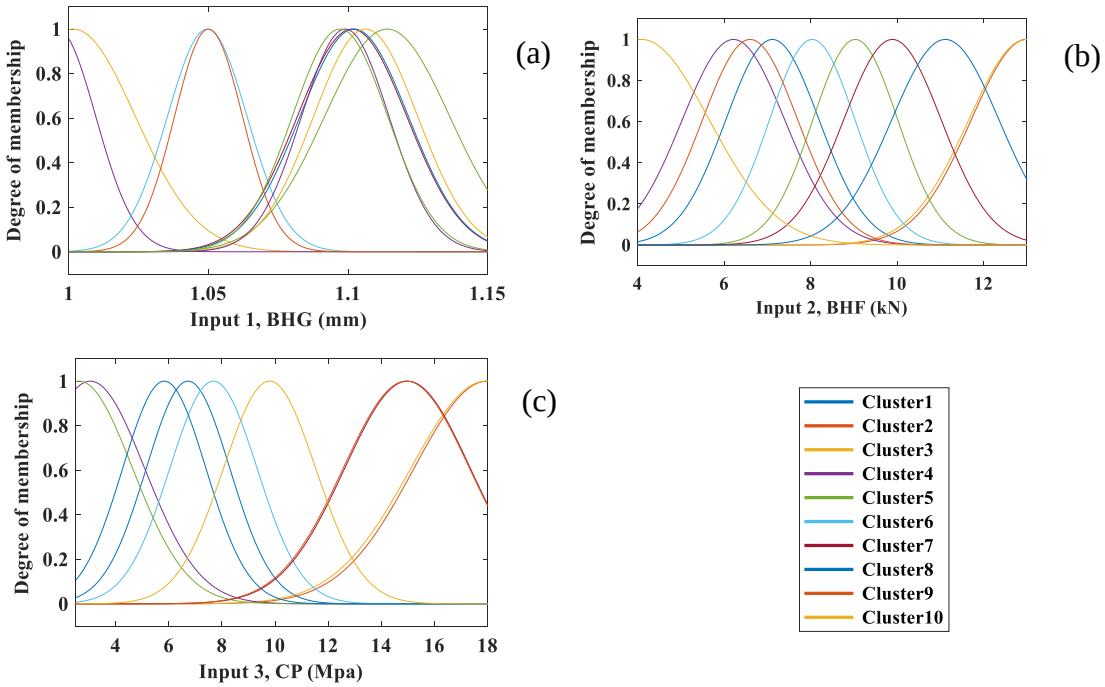

Fig. 10. Optimized membership functions for achieved depth; (a) Input 1, (b) Input 2 and (c) Input 3.

Metaheuristic algorithms are very parameter dependent; however, the gray wolf optimization algorithm, due to less adjustable parameters than other algorithms, shows less dependence on parameter variations. Also, in the application of metaheuristic algorithms in modeling, especially

in combination with other soft computational methods such as artificial neural networks and fuzzy inference systems, it cannot be claimed that the optimal result is found. However, by repeating the optimization process, one can be sure that the problem is not caught in the local minima. For this purpose, in the present study, with numerous simulations with changes in the input parameters of the algorithm, an attempt has been made to achieve the optimal ANFIS structure, although it cannot be said that this is the best possible structure.

Here are some graphical methods used to examine the efficacy of the present model. Fig. 11 displays the data approximated by the ANFIS model and the actual data simultaneously for each of the hydroforming process outputs. In these diagrams, the triangular symbols are associated with the data utilized in the training section, and the square symbols are related to the data in the test section. The middle $E = P$ is a reference to determine the accuracy of the attained network. It can be seen that the efficiency of the model is very high for predicting training data for all outputs. It can also be observed that the efficiency of the model for predicting the desired outputs is high. Next, Fig. 12 shows the value of aluminum thinning rate (upper layer and lower layer), the height of wrinkles, and the achieved depth of the hydroforming process for the predicted and actual data in both the testing and training sections. In particular, the red and blue lines are corresponding to the laboratory data, for the testing and training sections. Also, triangular and square symbols are corresponding to the data estimated by the model related to the training and testing section. As can be seen in these diagrams, the ANFIS grid corresponds to the training section data for all outputs (the triangular symbols correspond to the red lines). The second part of the diagrams also shows that the network is effective in predicting the data related to the test section.

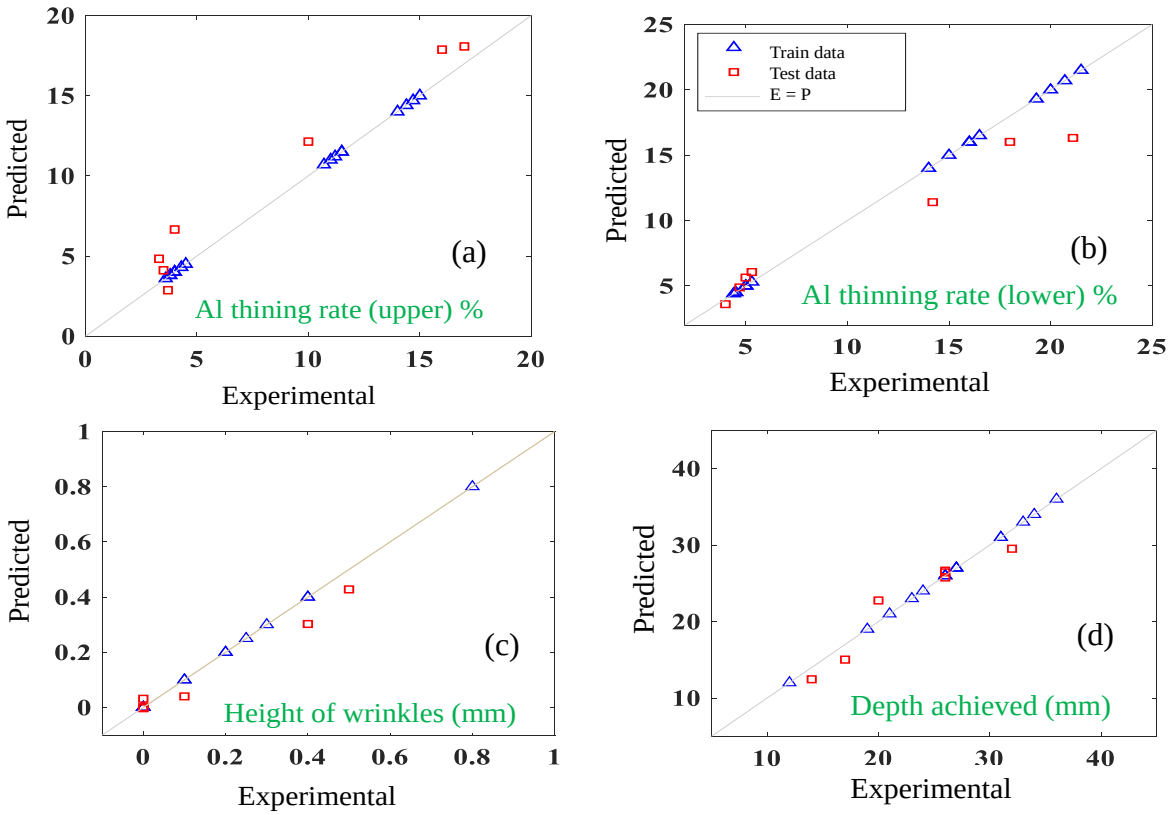

Fig. 11. Comparison between experimental data and prediction data for; (a) all thinning rate (upper), (b) all thinning rate (lower), (c) height of wrinkles and (d) depth achieved.

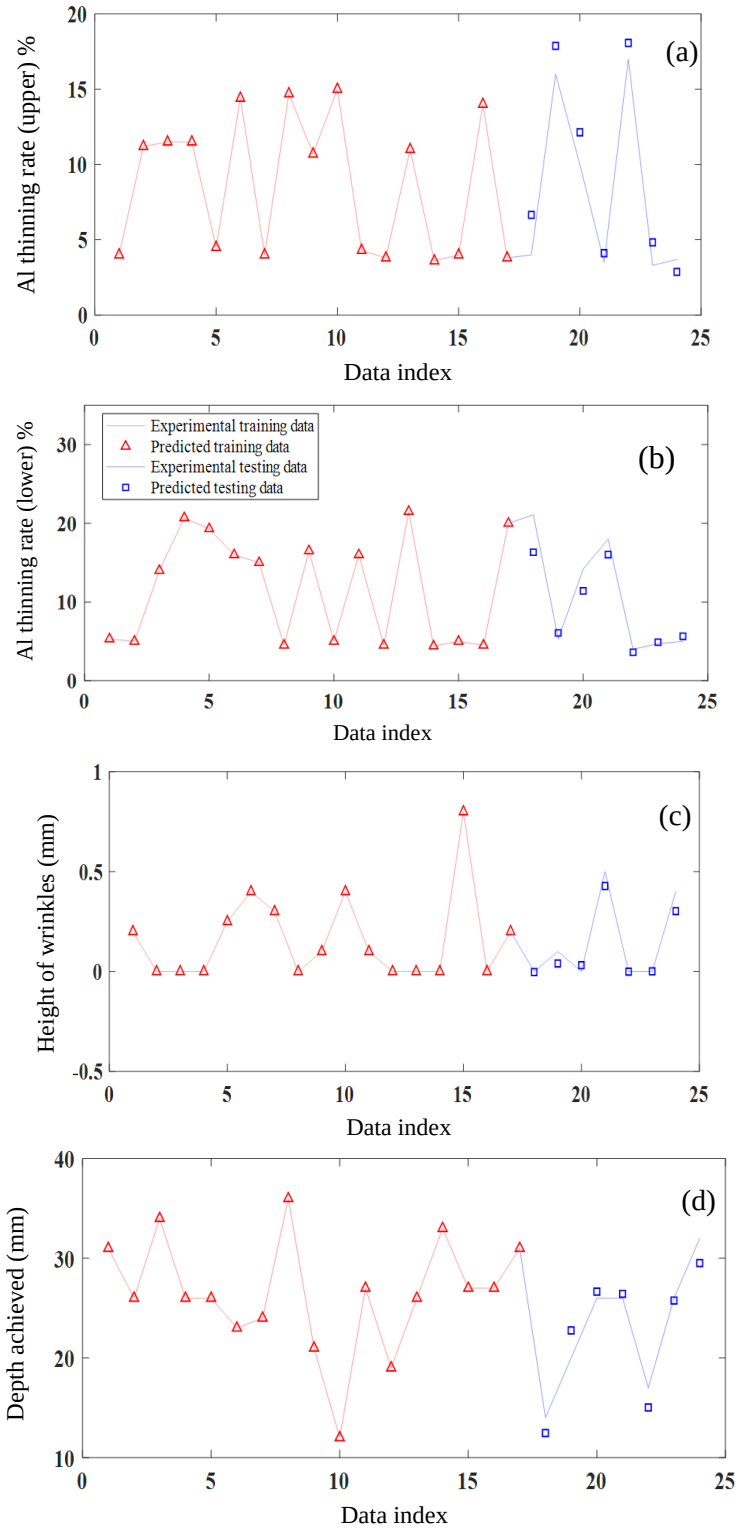

Fig. 12. Error of practical and predicted data for; (a) all thinning rate (upper), (b) all thinning rate (lower), (c) height of wrinkles and (d) depth achieved.

In order to quantitatively assess the precision of the attained model, the criteria of root mean square error, mean absolute error, and correlation coefficient have been used. How to calculate these criteria is presented in Eqs. (21-23), respectively.

$$RMSE = \sqrt{\frac{1}{n} \times \sum_{i=1}^{n} (O_A - O_P)^2} \quad (21)$$

$$MAE = \frac{1}{n} \sum_{i=1}^{n} |O_A - O_P| \quad (22)$$

$$R = \frac{\sum_{i=1}^{n} [(O_A - \bar{O}_A)(O_P - \bar{O}_P)}{\sqrt{\left[\sum_{i=1}^{n} (O_A - \bar{O}_A)^2\right]\left[\sum_{i=1}^{n} (O_P - \bar{O}_P)^2\right]}} \quad (23)$$

That in these relationships, O_A the amount of output measured for the sample i, O_P the output estimated by the model for the sample i,$\bar{O}_A$ the mean of the actual data, and $\bar{O}_P$ the mean of the approximated data. To check the precision of the model, the criteria have been computed for the testing and training parts to model hydroforming process and are listed in Table 5. It can be seen that the attained model has generally been effective in approximating all outputs of the hydroforming process.

Table 5. The RMSE, MAE, R, and MAE Criteria for modeling aluminum thinning rate (upper layer and lower layer), height of wrinkles and achieved depth.

		RMSE	MAE	R
Al thinning rate (upper) %	Train	1.02E-06	5.21E-07	1
	Test	1.676519	1.53	0.985
Al thinning rate (lower) %	Train	2.72E-05	1.36E-05	1
	Test	2.257774	1.647581	0.989
Height of wrinkles (mm)	Train	2.24E-09	1.34E-09	1
	Test	0.052491	0.037879	0.99
Depth achieved (mm)	Train	7.18E-06	3.82E-06	1
	Test	2.675977	2.09745	0.906

The *RMSE* and *MAE* criteria are very small, especially for the education sector. Of course, these criteria alone are not appropriate for evaluating the model. Next, *R* a criterion is used that shows the degree of conformity of the predicted data with the laboratory data. The correlation coefficient R for the education section is 1, which indicates the complete agreement of the laboratory data with the ANFIS data in the education department. The correlation coefficient for the test section is very high for all outputs (close to 1), which shows the high efficiency of the optimized model.

5. Conclusions

In this study, the ANFIS network optimized by the gray wolf optimization algorithm is to model the hydroforming process based on the input blank holder force, blank holder gap, and cavity pressure and output aluminum thinning rate (upper layer and lower layer), the height of wrinkles and the achieved depth variables. The results show that the optimized model is very effectual, and it is possible to approximate the values of aluminum thinning rate (upper layer and lower layer), the height of wrinkles and achieved depth based on changes in process input variables. The correlation coefficient *R* for modeling the process temperature values in the training section is 1 and for the test section is very close to one, which indicates a very good agreement between the results estimated by the network and the laboratory results. The results also show that the root means square error of four outputs of aluminum thinning rate, upper layer and lower layer, the height of wrinkles, and the achieved dept of the test section, are 1.67, 2.25, 0.05, and 2.67, respectively.

References

[1] E. C. Botelho, R. A. Silva, L. C. Pardini and M. C. Rezende, “A review on the development and properties of continuous fiber/epoxy/aluminum hybrid composites for aircraft structures”, *Mater. Res.*, Vol. 9, No. 3, pp. 247-256, (2006).

[2] T. Sinmazçelik, E. Avcu, M. Ö. Bora and O. Çoban, “A review: Fibre metal laminates, background, bonding types and

applied test methods", *Mater. Des.*, Vol. 32, No. 7, pp. 3671-3685, (2011).

[3] L. B. Vogelesang and A. Vlot, "Development of fibre metal laminates for advanced aerospace structures", *J. Mater. Process. Technol.*, Vol. 103, No. 1, pp 1-5, (2000).

[4] T. Takamatsu, T. Matsumura, N. Ogura, T. Shimokawa and Y. Kakuta, "Fatigue crack growth properties of a GLARE3-5/4 fiber/metal laminate", *Eng. Fract. Mech.*, Vol. 63, No. 3, pp. 253-272, (1999).

[5] J. Carrillo and W. Cantwell, "Mechanical properties of a novel fiber–metal laminate based on a polypropylene composite", *Mech. Mater.*, Vol. 41, No. 7, pp. 828-838, (2009).

[6] T. Takamatsu, T. Shimokawa, T. Matsumura, Y. Miyoshi and Y. Tanabe, "Evaluation of fatigue crack growth behavior of GLARE3 fiber/metal laminates using a compliance method", *Eng. Fract. Mech.*, Vol. 70, No. 18, pp. 2603-2616, (2003).

[7] J. Homan, "Fatigue initiation in fibre metal laminates", *In.t J. Fatigue.*, Vol. 28, No. 4, pp. 366-374, (2006).

[8] A. Volt, L. Vogelesang and T. De Vries, "Towards application of fiber metal laminates in larger aircraft", *Aircr. Eng. Aerosp. Technol.*, Vol. 71, No. 6, pp. 558-570, (1999).

[9] S. Suresh and V. S. S. Kumar, "Investigation on influence of stamp forming parameters on formability of thermoplastic composite", *Ass. Bra. Pol.*, Vol. 28, No. 5, pp. 422-432, (2018).

[10] H. Friedrich and S. Schumann, "Research for a new age of magnesium in the automotive industry" *J. Mater. Process. Technol.*, Vol. 117, No. 3, pp. 276-281, (2001).

[11] H. Kang and G. Reyes-Villanueva, "Fatigue prediction of lightweight thermoplastic fiber-metal laminates", *J. Test. Eval.*, Vol. 35, No. 3, pp. 266-71, (2007).

[12] R. Zhang, L. Lang, R. Zafar, L. Lin and W. Zhang, "Investigation into thinning and spring back of multilayer metal forming using hydro-mechanical deep drawing (HMDD) for lightweight parts", *Int. J. Adv. Manuf. Technol.*, Vol. 82, No 5-8, pp. 817-826, (2016).

[13] R. Zhang, L. Lang and R. Zafar, "FEM-based strain analysis study for multilayer sheet forming process", *Front. Mech. Eng.*, Vol. 10, No. 4, pp. 373-379, (2015).

[14] R.-j. Zhang, L.-h. Lang, R. Zafar, L. Kui and W. Lei, "Effect of gap generator blank thickness on formability in multilayer stamp forming process", *Trans. Nonferrous. Met. Soc. China.*, Vol. 26, No. 9, pp. 2442-2448, (2016).

[15] L. C. Chan and W. K. R. Kot, "Determination of loading paths in warm hydroforming reinforced quadrilateral tubular components", *Mater. Manuf. Process.*, Vol. 29, No. 1, pp. 32-36, (2014).

[16] R. Gerlach, C. R. Siviour, J. Wiegand and N. Petrinic, "The strain rate dependent material behavior of S-GFRP extracted from GLARE" *Mech. Adv. Mater. Struct.*, Vol. 20, No. 7, pp. 505-514, (2013).

[17] Z.-J. Wang, L. Yi, J.-g. Liu and Y.-H. Zhang, "Evaluation of forming limit in viscous pressure forming of automotive aluminum alloy 6k21-T4 sheet", *Trans. Nonferrous. Met. Soc. China.*, Vol. 17, No. 6, pp. 1169-1174, (2007).

[18] J. P. M. Correia and S. Ahzi, "Electromagnetic sheet bulging: analysis of process parameters by FE simulations", *Key. Eng. Mater.*, Vol. 554-557, pp. 741-748, (2013).

[19] E. Sherkatghanad, L. Lang, S. Liu and Y. Wang. "Innovative approach to mass production of fiber metal laminate sheets", *Mater. Manuf. Process.*, Vol. 33, No. 5, pp. 552-563, (2018).

[20] M. M. Thomas, B. Joseph and J. L. Kardos "Experimental characterization of autoclave-cured glass-epoxy composite laminates: Cure cycle effects upon thickness, void content, and related phenomena", *Polym. Compos.*, Vol. 18, No. 3, pp. 283-299, (1997).

[21] J. Yanagimoto and K. Ikeuchi, "Sheet forming process of carbon fiber reinforced

plastics for lightweight parts", *CIRP. Ann.*, Vol. 61, No. 1, pp. 247-250, (2012).

[22] T. Yokozeki, Y. Iwahori, S. Ishiwata and K. Enomoto, "Mechanical properties of CFRP laminates manufactured from unidirectional prepregs using CSCNT-dispersed epoxy Composites", *Compo.s Part A. Appl. Sci. Manuf.*, Vol. 38, No. 10, pp. 2121-2130, (2007).

[23] L. Mosse, P. Compston, W. J. Cantwell, M. Cardew-Hall and S. Kalyanasundaram, "Stamp forming of polypropylene based fibre–metal laminates: the effect of process variables on formability", *J. Mater. Process. Technol.*, Vol. 172, No. 2, pp. 163-168, (2006).

[24] L. Mosse, W. J. Cantwell, M. Cardew-Hall, P. Compston and S. Kalyanasundaram, "A study of the effect of process variables on the stamp forming of rectangular cups using Fibre-Metal Laminate systems", *Adv. Mat. Res.*, Vol. 6-8, pp. 649-656, (2005).

[25] M. R. Abdullah and W. J. Cantwell, "The high-velocity impact response of thermoplastic–matrix fibre–metal laminates", *J. Strain. Anal. Eng. Des.*, Vol. 98, No. 7, pp. 432-443, (2012).

[26] A. Yaghoobi, M. Bakhshi-Jooybari, A. Gorji and H. Baseri, "Application of adaptive neuro fuzzy inference system and genetic algorithm for pressure path optimization in sheet hydroforming process", *Int. J. Adv. Manuf. Technol.*, Vol. 86, No. 9, pp. 2667-2677, (2016).

[27] S. Kumar, S. Dhanabalan and C. Narayanan, "Application of ANFIS and GRA for multi-objective optimization of optimal wire-EDM parameters while machining Ti–6Al–4V alloy", *SN. Appl. Sci.*, Vol. 1, No. 4, pp. 1-12, (2019).

[28] B. Podder, P. Banerjee, K.R. Kumar and N.B. Hui, "Development of ANFIS Model for Flow Forming of Solution Annealed H30 Aluminium Tubes", *Solid. State. Phenom.*, Vol. 261, pp. 378-385, (2017).

[29] Y. D. Asl, Y. Y. Woo, Y. Kim and Y. H. Moon, "Non-sorting multi-objective optimization of flexible roll forming using artificial neural networks", *Int. J. Adv. Manuf. Technol*, Vol. 107, No. 5, pp. 2875-2888, (2020).

[30] R. T. Esfahani, S. I. Golabi and Z. Zojaji, "Optimization of finite element model of laser forming in circular path using genetic algorithms and ANFIS", *Soft. Comput.*, Vol. 20, No. 5, pp. 2031-2045, (2016).

[31] K. Maji and G. Kumar, "Inverse analysis and multi-objective optimization of single-point incremental forming of AA5083 aluminum alloy sheet", *Soft. Comput.*, Vol. 24, No. 6, pp. 4505-4521, (2020).

[32] M. E. Khamneh, M. Askari-Paykani, H. Shahverdi, S. M. M. Hadavi and M. Emami, "Optimization of spring-back in creep age forming process of 7075 Al-Alclad alloy using D-optimal design of experiment method", *Meas.*, Vol. 88, pp. 278-286, (2016).

[33] M. Safari, M. Salamat-Talab, A. Abdollahzade, A. Akhavan-Safar and L. da Silva, "Experimental investigation, statistical modeling and multi-objective optimization of creep age forming of fiber metal laminates", *Proc. Inst. Mech. Eng. Part L.*, Vol. 234, No. 11, pp. 1389-1398, (2020).

[34] S. Mirjalili, S.M. Mirjalili and A. Lewis, "Grey wolf optimizer", *Adv. Eng. Softw.*, Vol. 69, pp. 46-61, (2014).

How to cite this paper:

J. Akbari, H. Valaei and M. F. Sepahvand, " Numerical response using finite strip element including drilling degree of freedom,", *J. Comput. Appl. Res. Mech. Eng.,* Vol. 12, No. 2, pp. 193-209, (2023).

DOI: 10.22061/JCARME.2022.8268.2101

URL: https://jcarme.sru.ac.ir/?_action=showPDF&article=1708